

Broadband Spectroscopy during the Total Solar Eclipse of March 29, 2006

Sarah A. Jaeggli

Advisors: Shadia Habbal, Jeff Kuhn

ABSTRACT

The eclipse of March 29, 2006 attracted the University of Hawaii eclipse team to the desert plateau near Waw an Namus, Libya. The eclipse was successfully observed with three experiments. One of these experiments, a broadband spectrometer, was entirely student designed, built, and run as part of the Astronomy 699 project. In this paper the details of the broadband spectrometer experiment and its results are outlined. The broadband spectrometer is a commercial fiber-fed spectrograph with wavelength coverage from 350 to 1120 nm and a small telescope for light collection. During the eclipse two positions in the corona at $1.25 R_{sun}$ and $5.75-8.25 R_{sun}$ were observed. Due to the experimental nature of the instrument, several issues were resolved experimentally and by using an atmospheric modeling facility, MODTRAN. A comparison of the spectra from the inner and outer corona implies a significant color difference between the outer corona and the inner corona and therefore the solar disk color. The thermal and scattering contributions of dust and the possibility for the existence of fluorescing silicon nanoparticles are discussed.

1. Introduction

The solar corona can be identified spectroscopically by three different parts: the K corona, the F corona, and the E corona. The K corona emits a smooth continuum, looking very much like a spectrally smoothed solar disk spectrum. The K corona is very optically thin and its opacity is derived from electron scattering. Electrons in the corona are very hot and the solar spectrum scatters from these electrons, wavelengths get shifted by the electron velocities, and the effect is a smooth continuum, but with roughly the same shape (or color) as its source spectrum. The E corona exists alongside the K corona. This component originates from hot, partially ionized atoms that have escaped the solar surface and are streaming along with their electrons in the solar wind. Elements such as calcium, iron, nickel, and magnesium have prominent emission lines in the E coronal spectrum. At a few solar radii out from the sun it is possible to see a scattered solar spectrum from dust grains of a zodiacal origin. This

is the F or Fraunhofer corona, so called because it scatters the solar disk spectrum without a redistribution in wavelength. The dust is fragile; nearer to the sun than about $4 R_{\text{solar}}$ the dust is sublimated away.

These delicate and dim components of the solar corona cannot often be observed from the ground. The inner K corona barely stands out against the daytime sky at a good observing site, but eclipses offer a unique opportunity to observe further out in the solar corona for a limited time when the sky dims by three orders of magnitude.

This experiment was opportunistic and was designed as a support instrument for the two other eclipse experiments. It was not geared to any one science goal. The purpose of this instrument was to look at the integrated corona at a particular radius and get a spectrum from the ultraviolet to the infrared for that position. The fact that it covered such a broad range of wavelengths and reached so much farther into the blue end of the spectrum has allowed it a unique result from the other two.

2. Experimental Setup

From the requirements above a very simple design was developed from commercial science-grade elements and components made in the lab. The spectrograph used in this project was a QE65000 from Ocean Optics with a $200 \times 1000 \mu\text{m}$ slit. The QE65000 is a high quantum efficiency spectrograph with a wavelength range spanning 350 to 1120 nm, from the near-ultraviolet to the near-infrared, but with the limited spectral resolution of about 0.75 nm per pixel. The spectrograph slit does not allow the distinction of spatial resolution. A higher optical efficiency is achieved by integrating the light from a line of pixels in the spatial direction, therefore the slit provides no spatial resolution and significantly increases the simplicity of the external optical system. For light collection, a spherical mirror of six inches diameter and f/1 focal length was used. Collection area and image size were selected over image quality. With this optic a field of view of $1.25 R_{\text{sun}}$ appears as 1.5 mm at the focal plane. A handmade fiber bundle bridged the gap between the mirror and the spectrograph. For the bundle a $145 \mu\text{m}$ diameter fiber with good transmission over the spectrograph range was selected. At prime focus 36 fibers were arranged in a circular annulus of 1.9 mm. With fibers of $145 \mu\text{m}$, the fiber bundle covers an annulus of 1.25 to 1.30 solar radii which was designed to cover the brightest part of the solar K corona without being too close to prominences near the limb. The end of the fiber at the focal plane is overpopulated by fibers, only about 14 fibers are able to fill the spectrograph slit. To protect the optics during solar disk observations and instrument focusing, a masking plate with a 0.05 inch hole could be slipped into the system just beyond prime focus. A digital video recorder was used to position

the telescope and record this position relative to the solar disk. The complete instrument without the mask is shown in figure 1.

3. Eclipse Observations

The eclipse site was chosen for having the best chance of good observing conditions and the longest duration of totality of all the possible sites. The site was positioned on a plateau near Waw an Namus, Libya, $24^{\circ}33'59.2''$ N, $17^{\circ}17'16.3''$ E, at an altitude of 439 m. A picture of the site is shown in figure 2. The eclipse occurred at 10:15 UT, 12:15 local time, on 29 March 2006 and was approximately 4^m06^s in duration. During this time period the broadband spectrograph recorded approximately 400 spectra at a 100 msec integration cadence with the fiber centered on the sun at a radius of $1.25 R_{solar}$ from the center of the solar disk and while the fiber was moved from the center to the field position. Then about 20 spectra were taken with an integration time of 10 sec with the fiber at the field position, covering 5.75 to $8.25 R_{solar}$. The fiber positions are shown in figure 3 with the correct angular size of the fiber with respect to the solar disk. The full unreduced time series of spectra taken during the eclipse is shown in figure 4. Bright segments of spectra represent where the was moved across a region with bright features near to the limb. In addition to these eclipse observations darks and calibration spectra of the solar disk and the sky were taken on site for future comparison.

4. Post-Observation Calibrations

There were several instrumental issues that needed to be identified and resolved during the analysis of this data that made it a particularly instructive project. As a student-built instrument system composed various commercial and hand built components, its performance was unknown and largely under-tested before the eclipse event. There are two particular effects observed in the eclipse data that have been recognized and studied in detail in post-event tests. These effects, their method of discovery, and their implications are provided in the following sub-sections in addition to other calibrations necessary for the reduction of the event data.



Fig. 1.— A picture of the instrument setup as reconstructed in the lab for one of the many post-eclipse tests. The spectrograph can be seen sitting next to the computer. The black fiber optic cable connects from prime focus to the spectrograph. The video camera is co-mounted with the telescope and shown with its solar filter on.



Fig. 2.— The site and observing tents on eclipse day near Waw an Namus, Libya.

4.1. Spectrograph Response

The spectrograph detector response as a function of wavelength was not initially known and was not quantitatively given by the manufacturer. Over such a large range at the peak of the solar energy output this information was needed to accurately represent the coronal flux. An uncontaminated spectrum of a source with a known wavelength dependence would have been quite difficult to obtain on site before or after the event. However it was possible to do this calibration in the lab under dark conditions. For calibration, an Ocean Optics halogen lamp with an approximate blackbody temperature of 3100 K was used. Spectra of the source were taken in a similar way to the eclipse observations. A median lamp spectrum was compiled and smoothed. A blackbody spectrum of 3100 K was calculated and divided from the smoothed lamp spectrum, leaving the response of the detector in arbitrary units. The lamp spectrum and blackbody together and the resulting response are shown in figure 5.

The response of the detector has been divided out in all the reduced data. This method was validated by comparing the solar disk spectrum with a model spectrum of the disk provided in Solar Astrophysics (Foukal 1990).

4.2. Line Aliasing

A more serious issue appeared when identifying what seemed to be red-shifted components of bright emission lines showing up in the sections of spectra dominated by prominences. An example of such a spectra is shown in figure 6. The trick was to determine if these components were instrumental artifacts or real, implying a velocity red-shift of 3000 km/s. The very fastest CMEs observed have reported velocities of 2500 km/s (Raymond et al.). This issue was quickly put to rest with the following test. An argon line source was positioned in front of the fiber end and a rotating slit was placed on this end, making it possible to select just a few fibers at once. When certain fibers were selected the argon spectra was observed to shift from some “rest” position to either red or blue. Examples of the argon “rest” spectrum and of one showing multiple components, this one blue shifted, are shown in figure 7. The multiples of strong emission lines are obviously an instrumental effect and knowing something of how the fiber bundle and spectrograph fit together helps to explain this effect. The spectrograph has a wide slit and the fiber size is slightly smaller, in fact two fibers can fit across the width of the slit almost side by side. In addition, the spectrograph end of the fiber was not polished. Even though the fiber ends were precision cleaved and inspected under a microscope, the ends were not perfectly flat, causing the light to exit the fibers at slightly randomized angles. These effects together are more than enough

to account for the shift in wavelength and the separate line components.

In this case there is no correction that can be applied. With these lines identified we can simply ignore them and assume that the other parts of the inner corona, the non-prominence positions, represent the “rest” position in the spectrograph and do wavelength calibration based on where these lines appear to be centered.

4.3. Identification of the Blue Excess

Another troubling problem similar in nature to the last one is a blue excess that appeared when observations of the solar disk were compared with those of the sky or corona and appeared regardless of geographical location. A division of the sky or coronal spectra by the solar disk spectra revealed a very large blue excess in the sky or coronal spectrum (or a deficit in the solar spectrum). The sky naturally appears bluer than the sun because of Rayleigh and Mie scattering in the atmosphere. To determine exactly how blue the sky should be when compared to the solar disk we used the moderate spectral resolution atmospheric transmittance algorithm and computer model (MODTRAN). The color differences given by the observed near and far corona divided by the solar disk spectrum in figure 8 are quite different from the modeled sky divided by the solar disk spectrum shown in figure 9. The observed spectra are much bluer than those modeled. Now why is this?

In post-eclipse observations in Hawaii, spectra of the solar disk and of the sky about 30 degrees away also showed this blue excess, however spectra taken with a different Ocean Optics spectrograph, but with the same fiber and other setup, showed no significant blue excess. Observations from the USB2000 and the QE65000 taken on the same day are compared in figure 10. This is unquestionably an instrumental effect. The other spectrograph is not high quantum efficiency, but has slightly finer resolution due to a narrower slit.

We believe that the interaction of the telescope mask, used when the telescope is pointed at the sun, the wide slit of the QE65000 spectrograph, and the refraction properties of the fiber bundle are the cause of the blue excess. With the mask on the fiber bundle receives a narrow range of angles from the telescope. Small entrance angles in the bundle mean small exit angles and little color dependency in refraction. When the mask is off of the telescope, as during totality or sky measurements, the fiber bundle receives light at the maximum of acceptance angle which is determined by the criterion for total internal refraction. Large entrance angles into the fiber bundle mean large exit angles at the other end and a greater effect of the color dependence of refraction. Blue light is refracted at larger angles than red light for the same input angle which means that fibers which do not fall on the slit but fall near

to it would contribute more blue light than red light, leading to a false color detection. The implication of this effect is that the color of masked and unmasked observations cannot be compared. Unmasked observations can only be compared with other unmasked observations, a fact which proves useful when looking at the color of the outer corona compared to that of the inner corona.

5. Data Reduction

Data reduction was done in a typical way. Darks were subtracted from all spectra. The spectrograph detector response described in section 4.1 was divided from all spectra creating the time series in figure 11. In order to more clearly see the emission lines a median smoothed spectra was subtracted from the response corrected spectra, creating the time series of spectra in figure 12. The flux differences caused by differences in integration time and whether or not the mask was present were removed and flux units were normalized to the peak flux of the solar disk. Due to the irregularity of the fibers, these flux units may contain errors up to an order of magnitude, although this does not appear to be the case as these unit agree with brightness measurements of the solar corona from past eclipses. The wavelength range of the spectrograph is shown reduced in these and all following spectra; the infrared sensitivity of the spectrograph is very low and nothing of interest appears beyond 900 nm.

6. Results

Line identifications shown at the top of figure 13 were made with data from the very beginning of the eclipse when there was a wealth of emission lines from solar activity near the limb. Surprisingly Ca II emission at 854.2 nm, a well known chromospheric line used in magnetograms, appears at the very beginning of the eclipse then appears again in absorption in the F corona spectrum. Many of the emission lines fade as more and more of the active corona is occulted by the lunar disk. It should be noted that many of the iron lines, though they are not very bright, do not fade throughout the eclipse. The spectra from these lines are shown at the bottom of figure 13. The source of these lines is not in prominences and activity near the limb, but further out and in a fairly even distribution in the corona.

The coronal spectrum in figure 14 was constructed from a median of sequence numbers 170-250 from the time sequence figures where the coronal spectrum was flat and regular. Absorption bands mostly of O₂ from the atmosphere are easy to distinguish from the smooth

continuum. The emission line spectrum at the bottom of figure 13 was made from a flattened, atmosphere subtracted version of this spectrum.

The coronal spectrum figure 15 is representative of the spectra from fiber position 2 and is a median of sequence numbers 410-430 in the time series. This spectrum has almost the same general shape as the position 1 spectrum but the jagged Fraunhofer absorption lines are very apparent and difficult to distinguish from the atmospheric absorption bands by itself. Comparing this spectra to the line identifications and the flattened spectra, we can see that $H\alpha$ and $Ca II$ lines from the reflected solar photosphere are visible.

The solar disk and sky spectra shown in figure 16 and 17 respectively are medians of about 100 spectra selected from the pre-eclipse calibration data. The solar disk spectrum appears to have a very different shape, especially in the 500 to 800 nm range, from either of the coronal positions. There is a linear drop off the red tail of the emission, whereas the coronal spectrum have some curvature here; this is the manifestation of the color problem discussed in section 4.3. The sky spectrum looks more similar to the coronal spectra but there is a secondary hump which is most probably due to dust reddening in the local atmosphere as this hump is not present in any of the Hawaii test data.

The color difference between the solar spectrum and the dust scattered F corona is modeled in Mann 1993. In this paper two components of reddening are discussed, reddening by forward scattering and reddening due to thermal emission by dust. Intensities at a longer wavelengths, 1000 or 2500 nm, are compared to the intensity at 500 nm where there is no reddening contribution from scattering. The ratio of the two intensities plotted against elongation is figure 1 in this paper. With the eclipse dataset it is possible to confirm the color result of the model F corona in Mann 1993. The phenomenon of the blue excess described in section 4.3 forbids comparison between the masked solar disk observations and the unmasked coronal observations, however the shape of the K corona is an analog for the solar spectrum and comparison between the spectra at the two positions is possible.

Comparison with the model requires that we extrapolate the “Reddening” inward to $1.25 R_{sun}$ in order to match the elongation of our observations. There is also some ambiguity in elongation of the observation at position 2, however reddening does not decrease much over the range of 6-8 R_{sun} . Values were picked and errors were associated with them. Values of the flux ratio at 500 and 1000 nm were obtained from the data shown in figure 18. comparing both ratios we see that the model falls within the error of these observations, however it fails to explain the rise in relative intensity at blue wavelengths and the change in slope at 800 nm.

7. Conclusions

This project has provided two broadband spectra from two unique positions in the corona with wavelengths reaching from the ultraviolet to the infrared for comparison to other eclipse data. It has also provided two sets of line identifications for early- and mid-eclipse alignments of the solar limb. There is a mysterious color result with few other results to compare with. The coronal model from Mann 1993 agrees with our result but does not well describe the color differences with wavelength especially the increase to the blue in the F corona. Other broadband observations made with different instruments of the F corona are needed in order to confirm this result.

I would like to thank Munir Nayfeh for the use of his nanoparticles and all the additional members of the Eclipse 2006 team for their invaluable help and support: Martina Arndt, Adrian Daw, Judd Johnson, Don Mickey, Huw Morgan, and Ilia Roussev. I would also like to thank Randy Chung for his patience and expertise during the design and construction process.

A. Appendix: Silicon Nanoparticles

The presence of silicon nanoparticles in the solar corona is still somewhat of a mystery. Li & Draine 2002 presented a study of nanoparticles in the interstellar medium. Models estimated the IR emission spectrum of the nanoparticles based upon their size and chemical components, which are basically broad(100 nm) spectral features with sharp peaks(10 nm) superimposed. In Habbal et al. 2003, the existence of dust grains is inferred from a source of extended IR emission in the corona which falls off less steeply than the observed behavior of the continuum. In addition this extended emission appears to be polarized tangentially to the solar limb as opposed to the nearby 1074.7 nm Fe XIII line which shows a radial polarization signature. Finally Rao et al. 2004, brought forth laboratory observations of silicon nanoparticles of 1 nm. Observations are made in the ultraviolet and show an upward slope of fluorescence starting from 400 nm to the ultraviolet for these particle sizes.

With silicon nanoparticle samples and a UV source it was possible to discover the flux distribution of the nanoparticles over a broad range of wavelengths by using a variety of instruments. Two nanoparticle samples were in solution with a solvent, tetrahydrofuran(THF) and isopropanol(ISO), in a glass sample container. The samples were illuminated such that only the fluorescence of the sample would be seen with no influence from the lamp seen in the detecting system. The nanoparticle samples were observed with the broadband spec-

trometer used in the eclipse and also using the Solar Eclipse Coronal Spectrograph built by Don Mickey with various detector ends: a 2k MCT array, a commercial grade InGaAs array, and a Princeton Instruments CCD sensitive into near infrared wavelengths. The visible wavelength spectra of both samples is shown in figure 19. As for the longer wavelength observations, there was no detection of additional infrared flux. The visible wavelength flux of the samples are accurately described by Gaussian distributions; THF with a peak at 650.5 and a FWHM of 61.6, and ISO with a peak at 678.9 and FWHM of 64.5.

No nanoparticle identifications have been made in the eclipse data based on the flux distribution seen here or those in the papers named above.

REFERENCES

- Anderson, J.M., Kieffer, H., & Becker, K., Modeling the Brightness of the Moon over 350-2500 nm for Spacecraft Calibration.
- Cram, L.E., 1976, Determination of the Temperature of the Solar Corona from the Spectrum of the Electron-Scattering Continuum, *Sol. Phys.*, 48, 3-19.
- Foukal, P.V., 1990, *Solar Astrophysics*.
- Habbal, S.R., et al., 2003, On the Detection of the Signature of Silicon Nanoparticle Dust Grains in Coronal Holes, *ApJ*, 592, L87-90.
- Kimura, H. & Mann, I., 1998, Brightness of the Solar F-Corona, *Earth Planets Space*, 50, 493-499.
- Li, A. & Draine, B.T., 2002, Are Silicon Nanoparticles and Interstellar Dust Component?, *ApJ*, 564, 803-812.
- Mann, I., 1992, The Solar F-Corona: Calculations of the Optical and Infrared Brightness of Circumsolar Dust, *A & A*, 261, 329-335.
- Mann, I., 1993, The Influence of Circumsolar Dust on the Whitelight Corona—Study of the Visual F-Corona Brightness, *Planet. Space Sci.*, 41, 301-305.
- Mann, I., et al., 2003, Dust Near the Sun, *Space Sci. Rev.*, 110, 269-305.
- Rao, S., et al., 2004, Excited States of Tetrahedral Single-core Si₂₉ Nanoparticles, *Phys. Rev. B*, 69.

Raymond, J.C., et al., 2003, Far-Ultraviolet Spectra of Fast Coronal Mass Ejections Associated with X-Class Flares, *ApJ*, 597, 1106-1117.

Reginald, N.R., Davaila, J.M., & St. Cyr, O.C., 2004, The Effects of Streamers on the Shape of the K-Coronal Spectrum, *Sol. Phys.*, 225, 249-265.

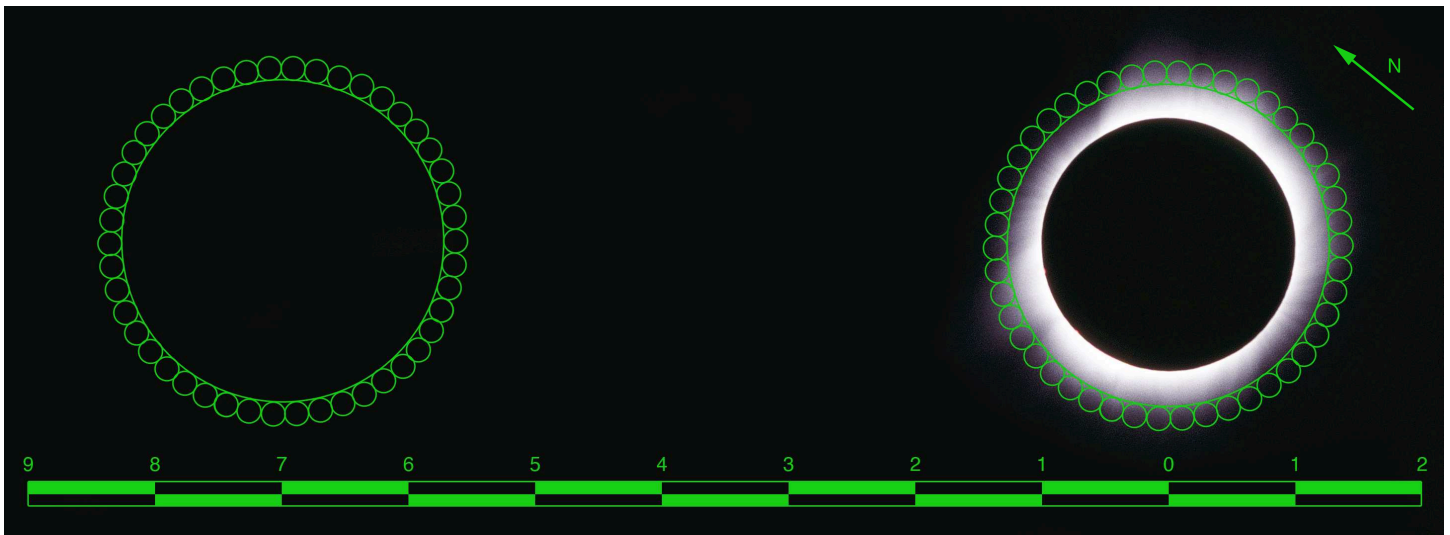


Fig. 3.— Showing the two positions of the fiber bundle with correct relative size compared to the solar disk, the initial position (1) is on the right and the final position (2) is on the left.

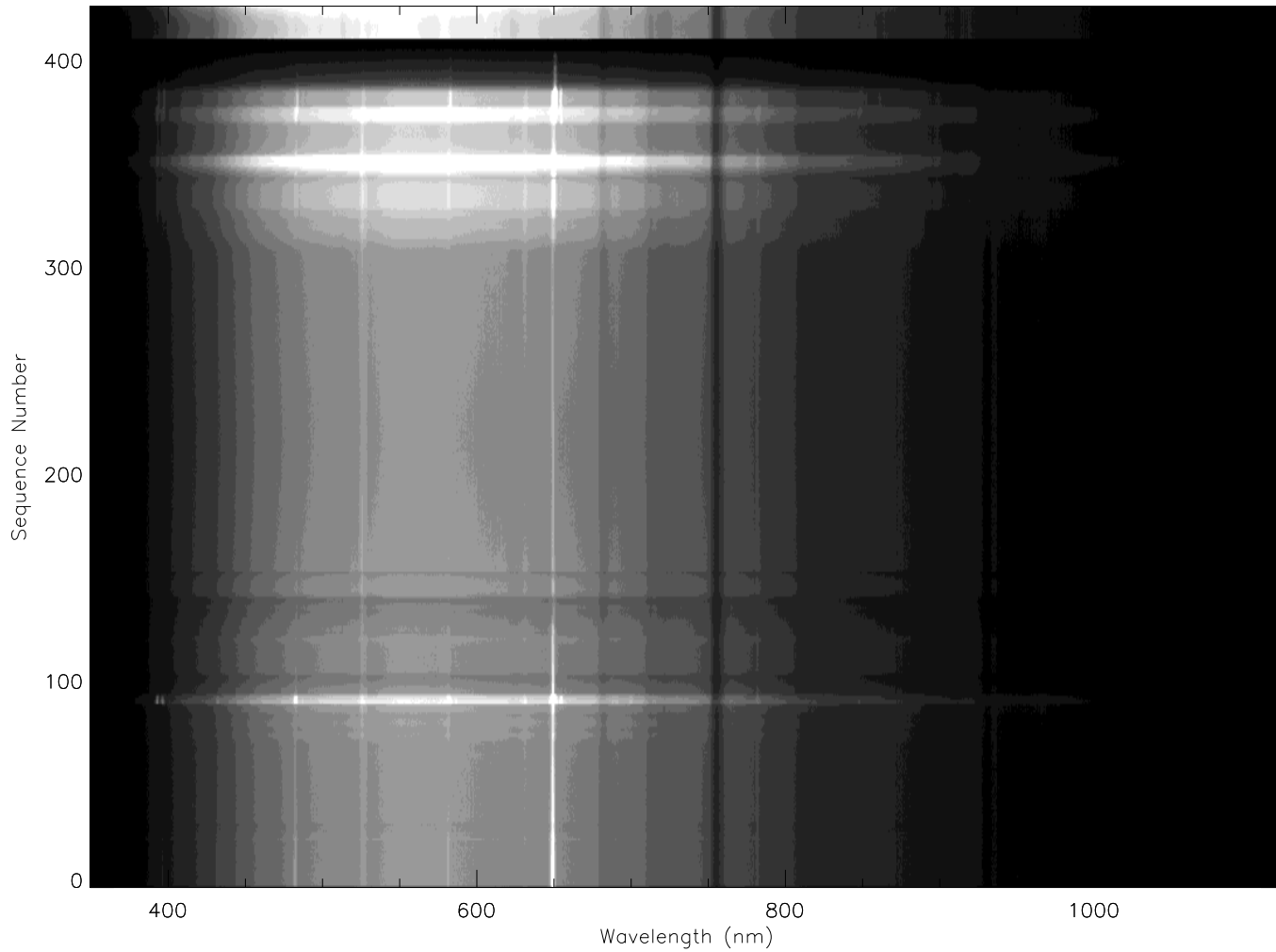


Fig. 4.— The raw time series of spectra from the day of the eclipse. Brightenings in the spectra indicate where prominence features near to the limb were included in the field of view.

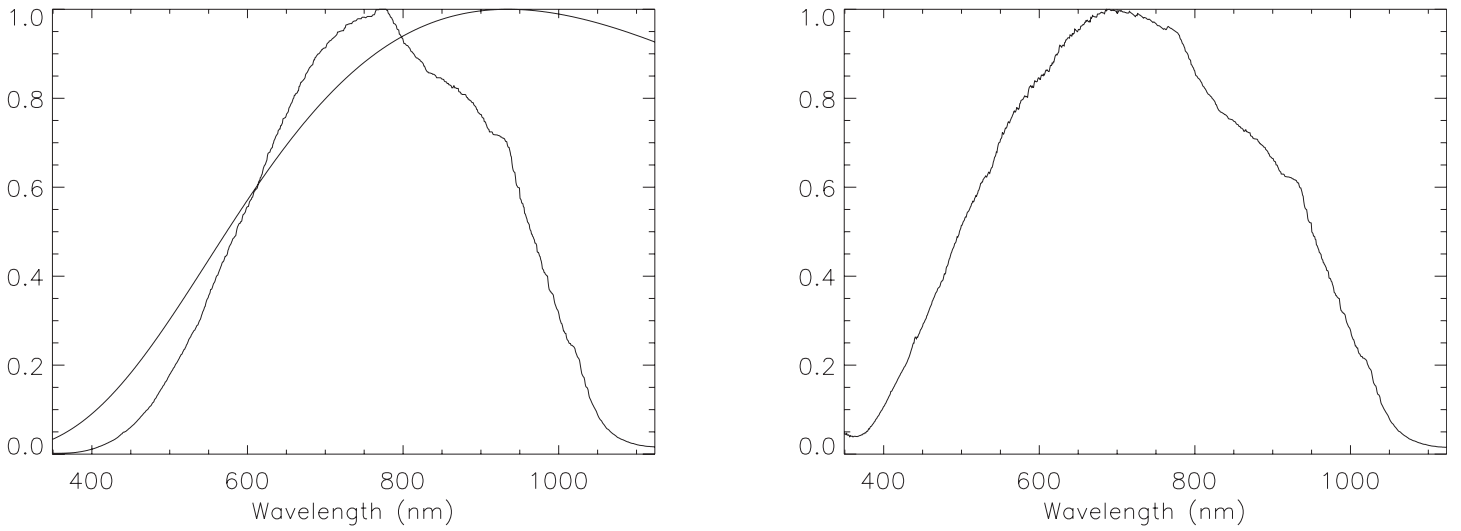


Fig. 5.— Spectrum of the halogen lamp and a scaled over-plotted blackbody spectrum of 3100 K (left), compared with the result of division, the spectrograph response with wavelength (right).

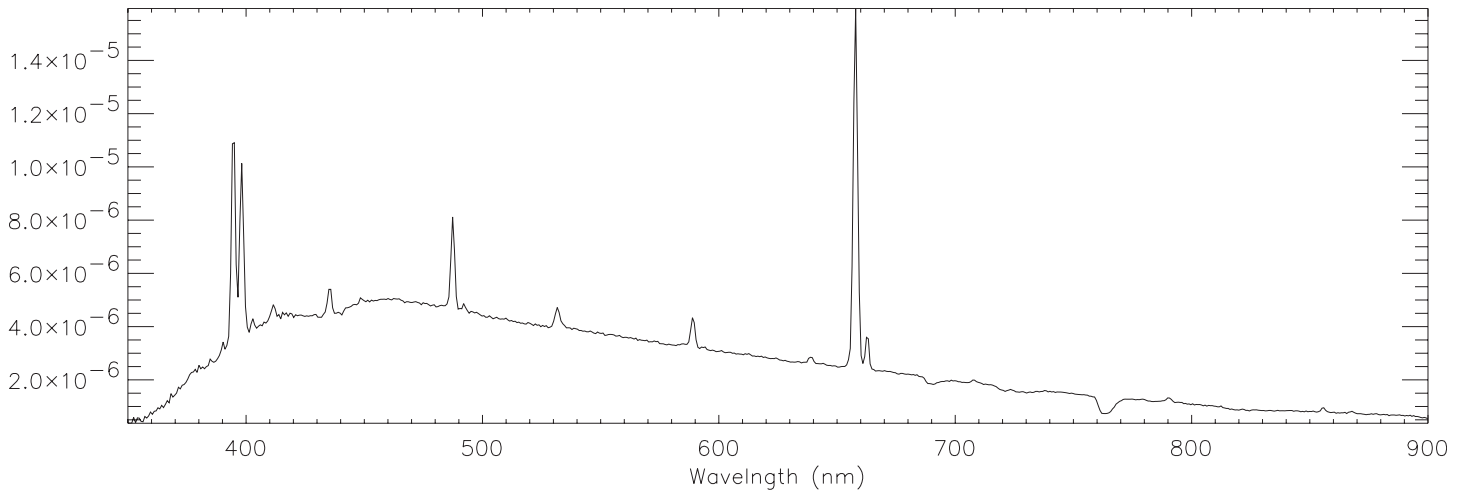


Fig. 6.— A spectrum from the first prominence dominated region, the H α and other strong lines clearly have two components.

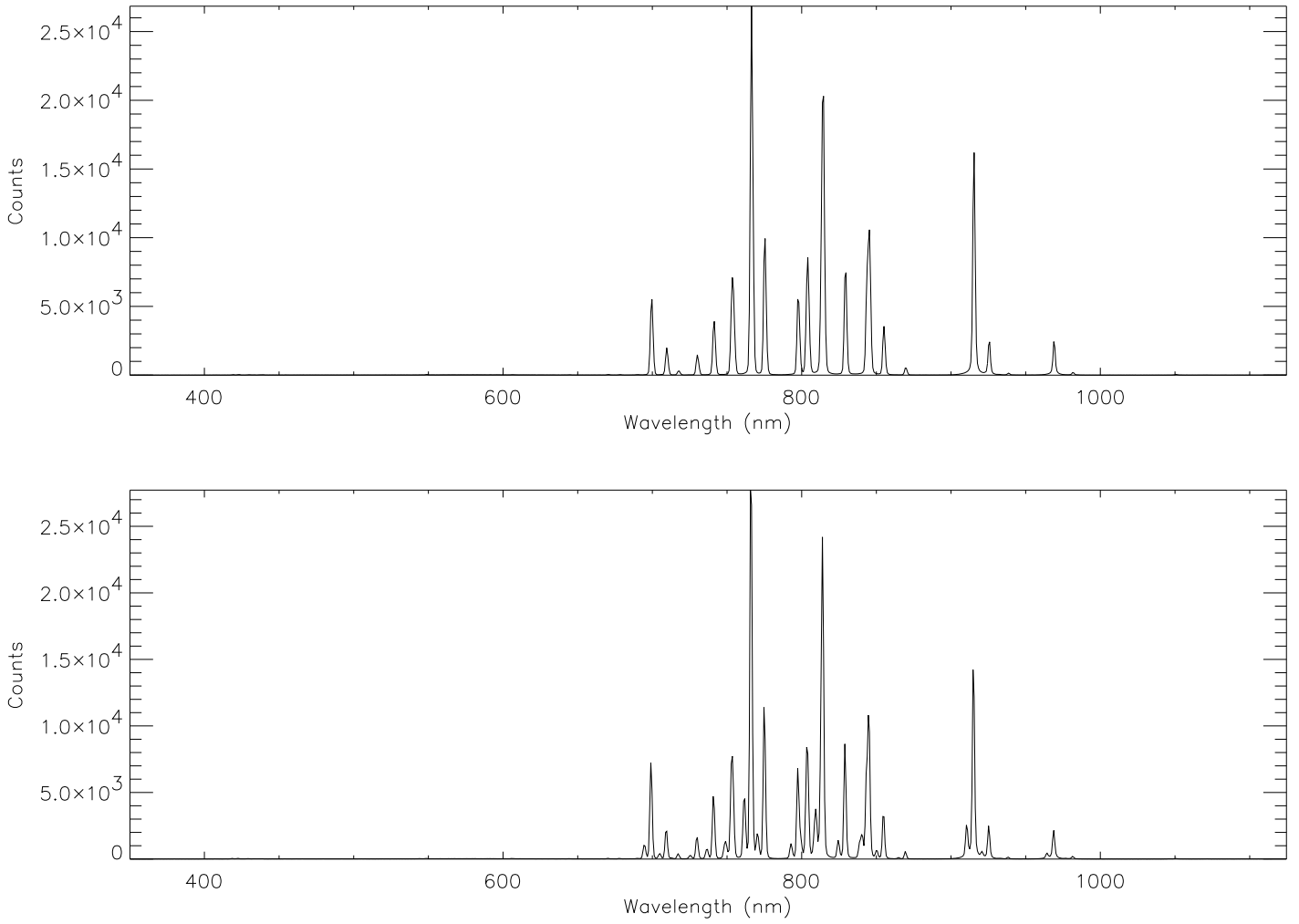


Fig. 7.— Two spectra from the argon-slit experiment where the spectra appears singly (top) and with multiple components at different wavelengths (bottom).

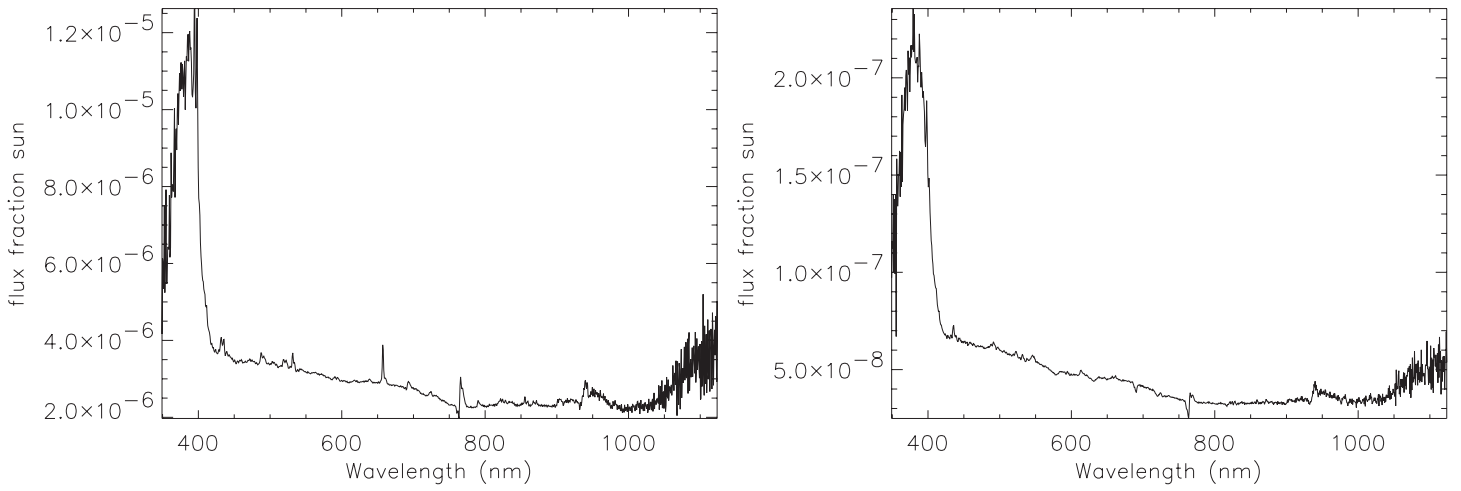


Fig. 8.— The average spectra at position 1 divided by the solar spectrum (left), and similarly for position two (right), revealing the unexpected blue color difference.

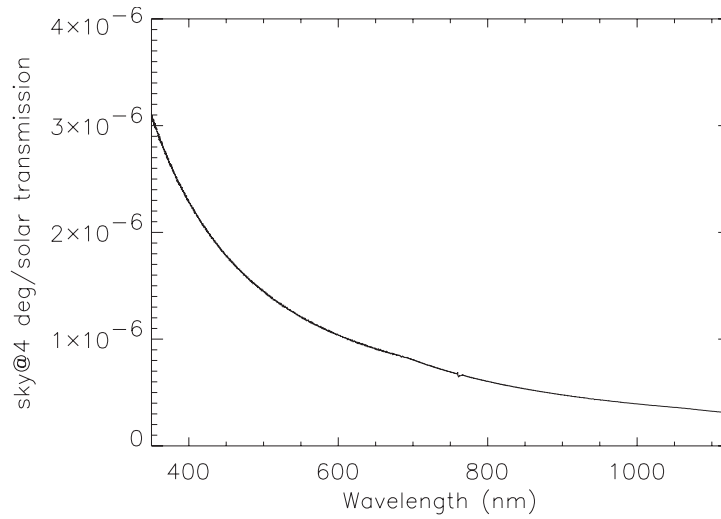


Fig. 9.— A plot from the MODTRAN model atmosphere shows the sky to sun flux fraction for a position four degrees from the solar disk.

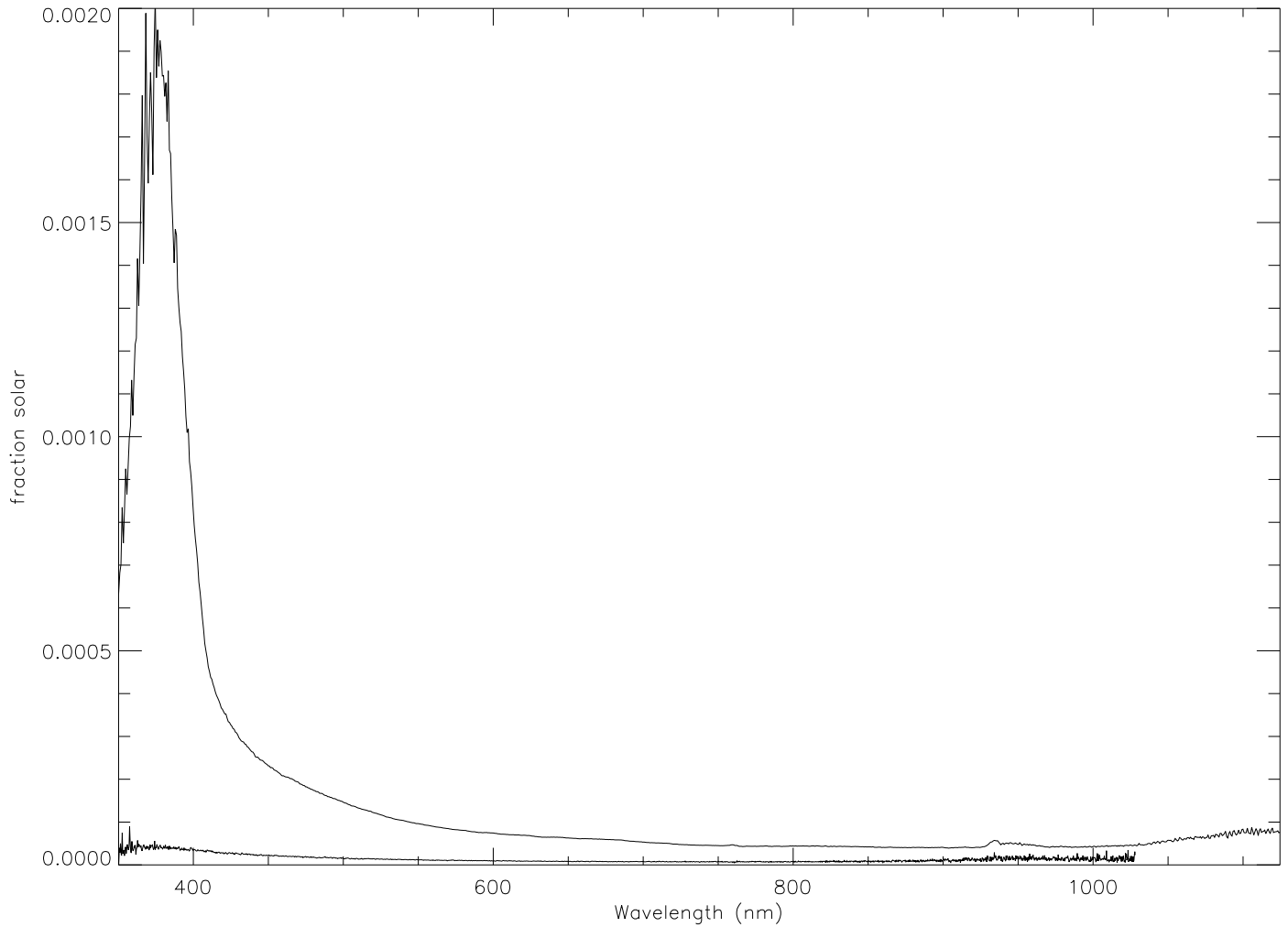


Fig. 10.— For the same positions on the sky and solar disk, the two spectrographs give conflicting results. The top curve is the division of a sky position about 30 degrees away from the sun by the solar disk spectrum taken by the QE65000 eclipse spectrograph, the bottom curve represents the same for the USB2000 spectrograph.

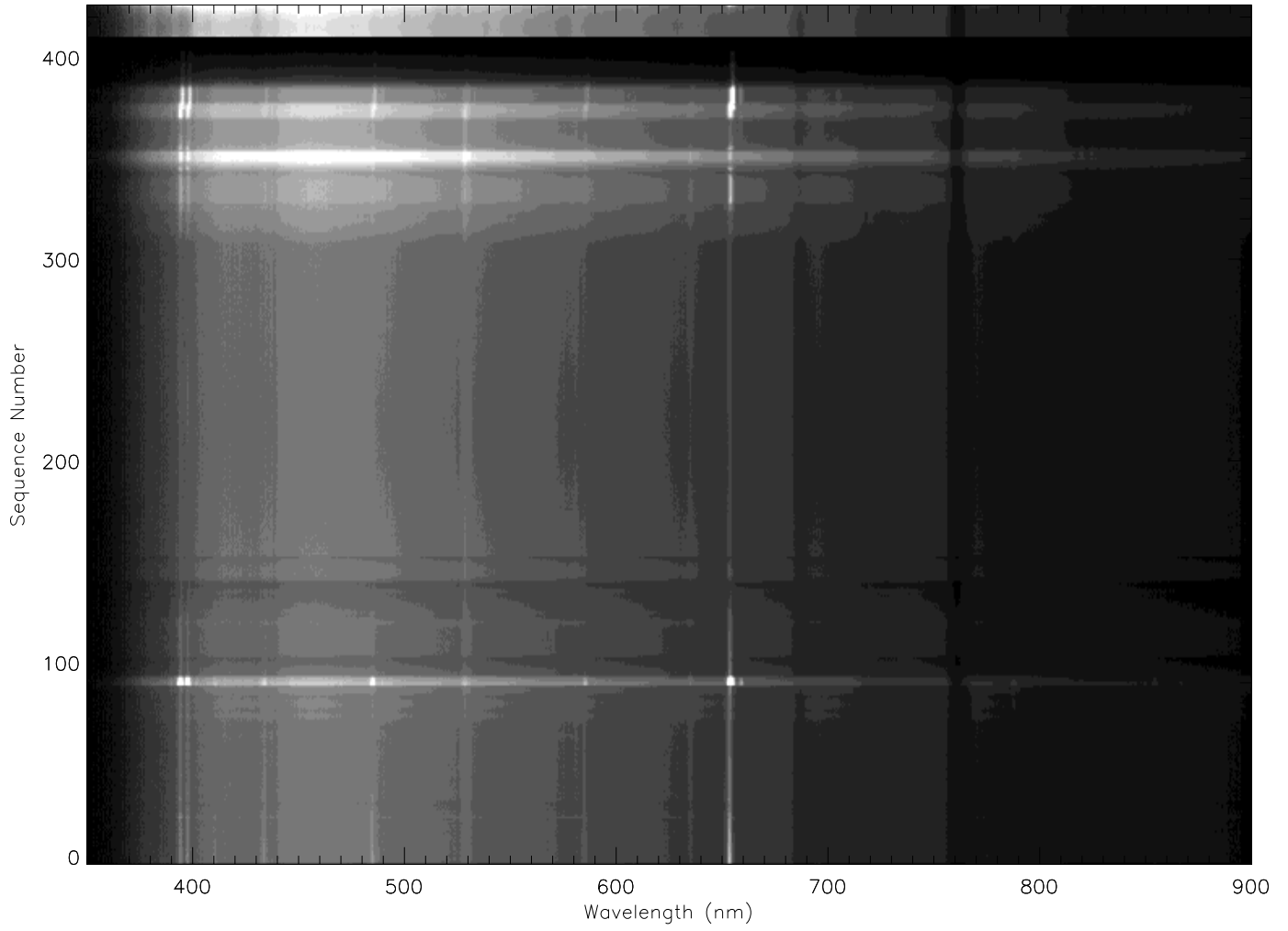


Fig. 11.— The time sequence of spectra in Figure 4 corrected for the spectrograph detector response.

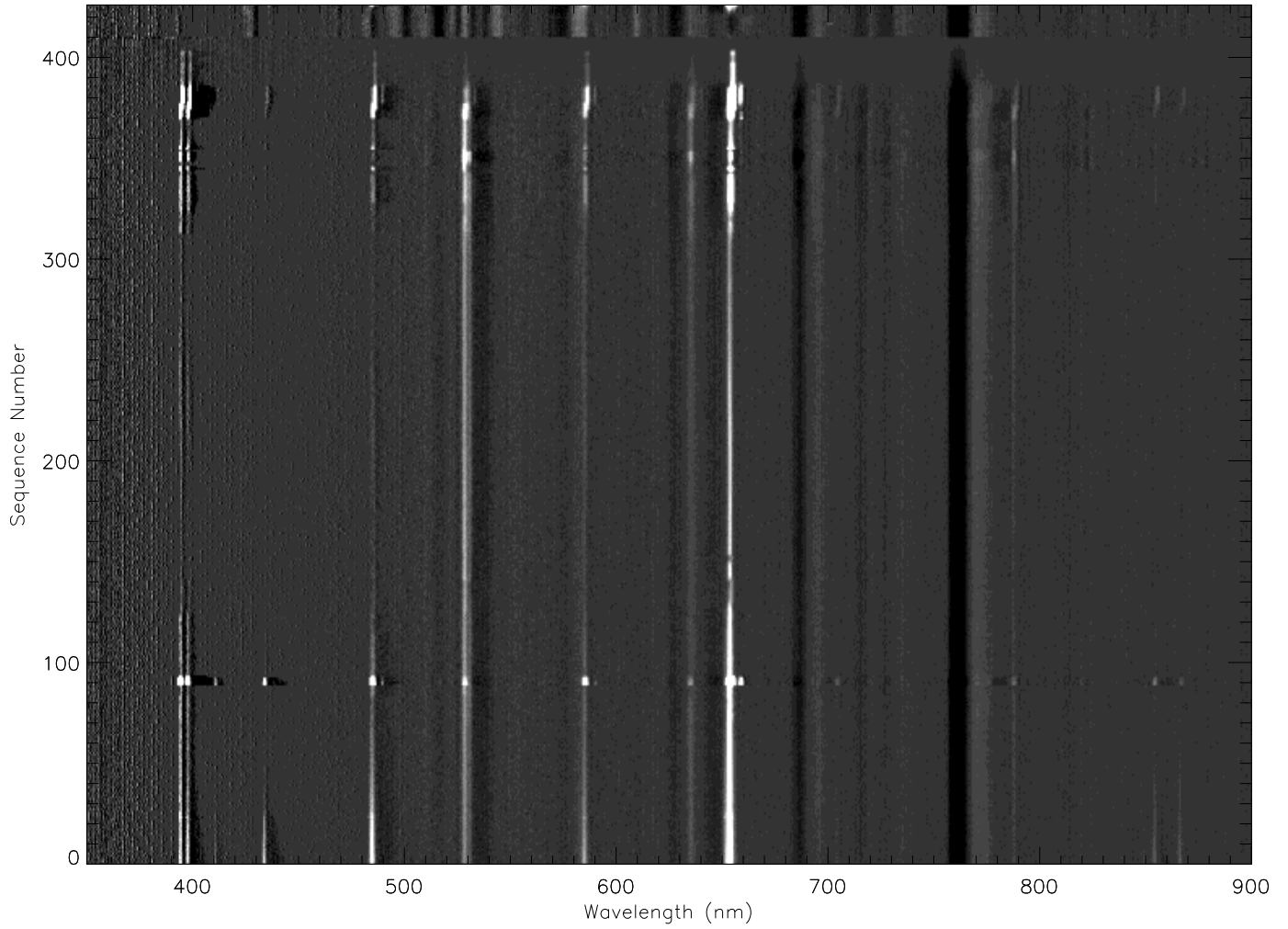


Fig. 12.— The time sequence of spectra in Figure 4 response corrected and flattened by subtracting a median smoothed spectrum from each row to show emission lines.

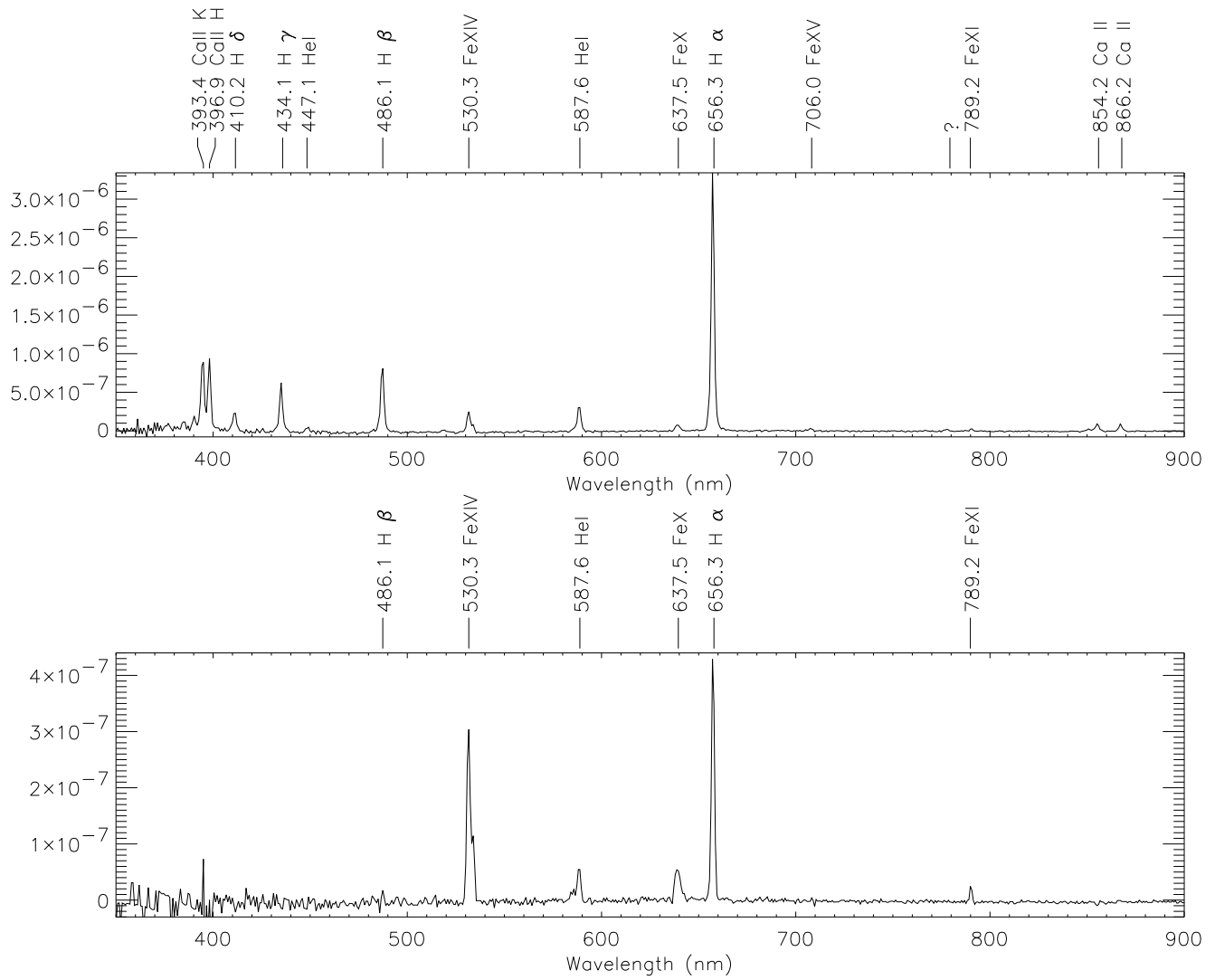


Fig. 13.— Two line spectra from position 1, one from the very beginning of the eclipse when the chromospheric lines are still very bright (top) and the second from a more advanced time when the chromospheric lines have disappeared (bottom).

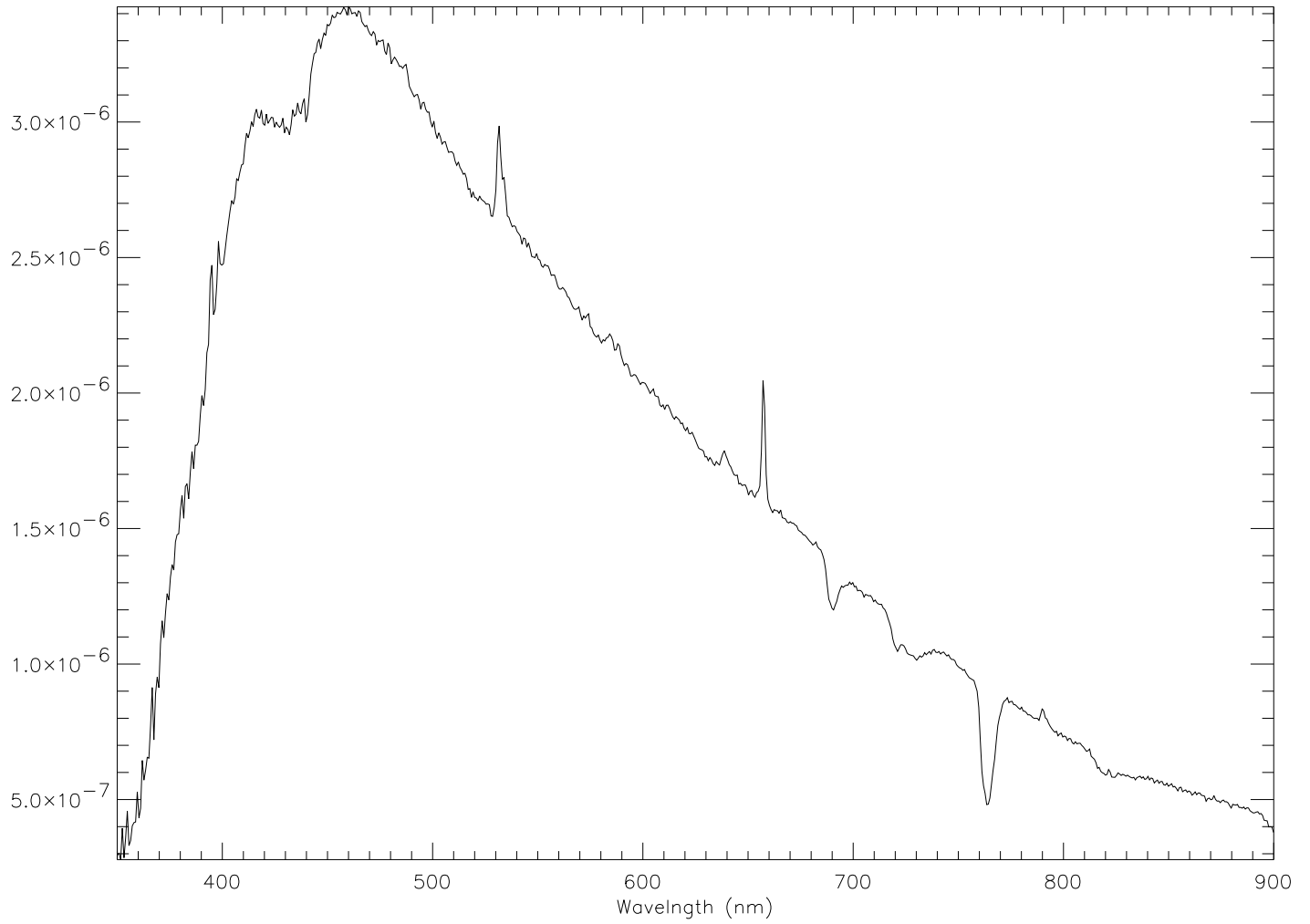


Fig. 14.— The average coronal spectrum at position 1 shows clear signatures of the K and E corona. Flux has been scaled by the maximum of the solar disk spectrum.

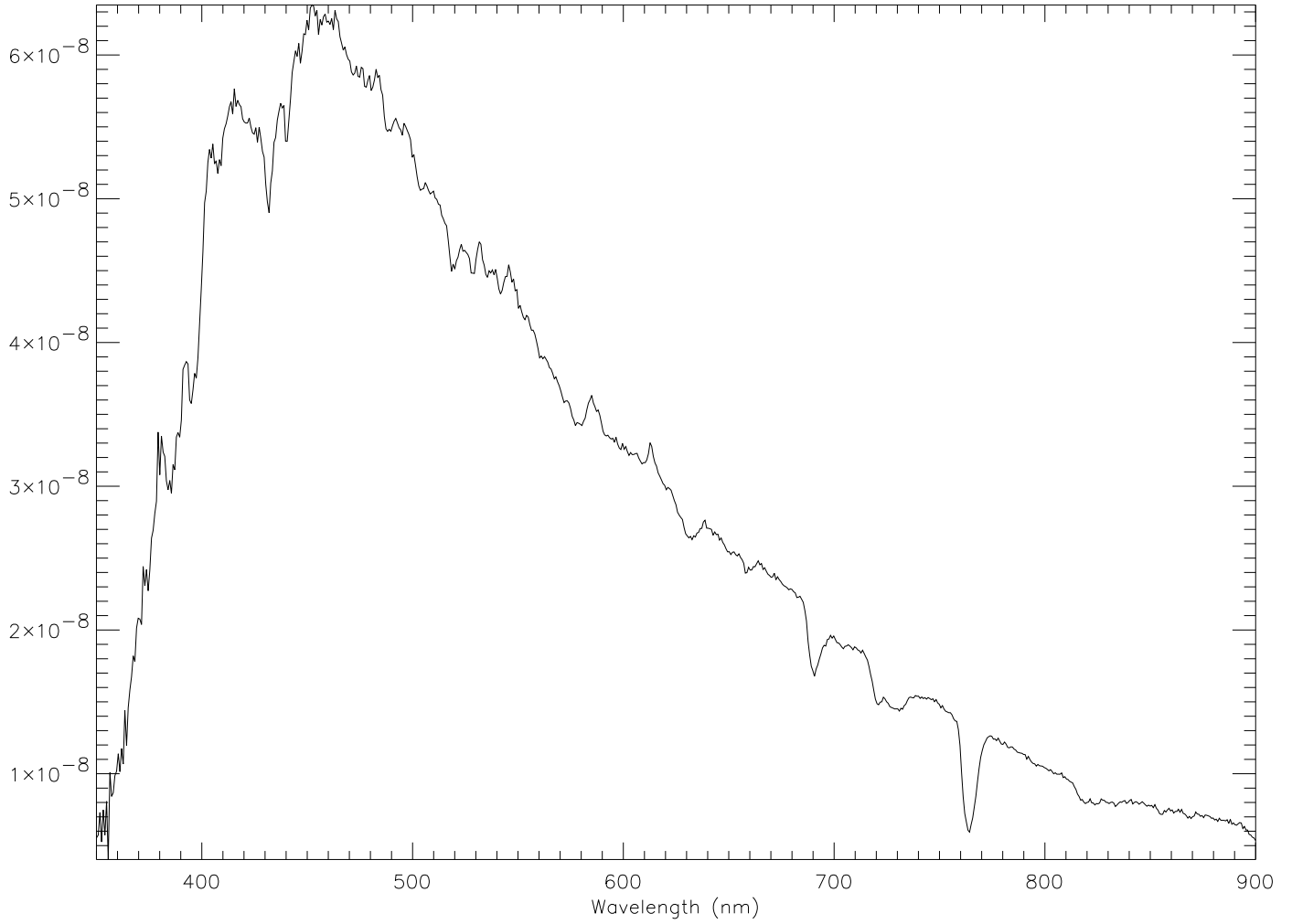


Fig. 15.— The average coronal spectrum at position 2 shows the jagged absorption features of the F corona. Flux has been scaled by the maximum of the solar disk spectrum.

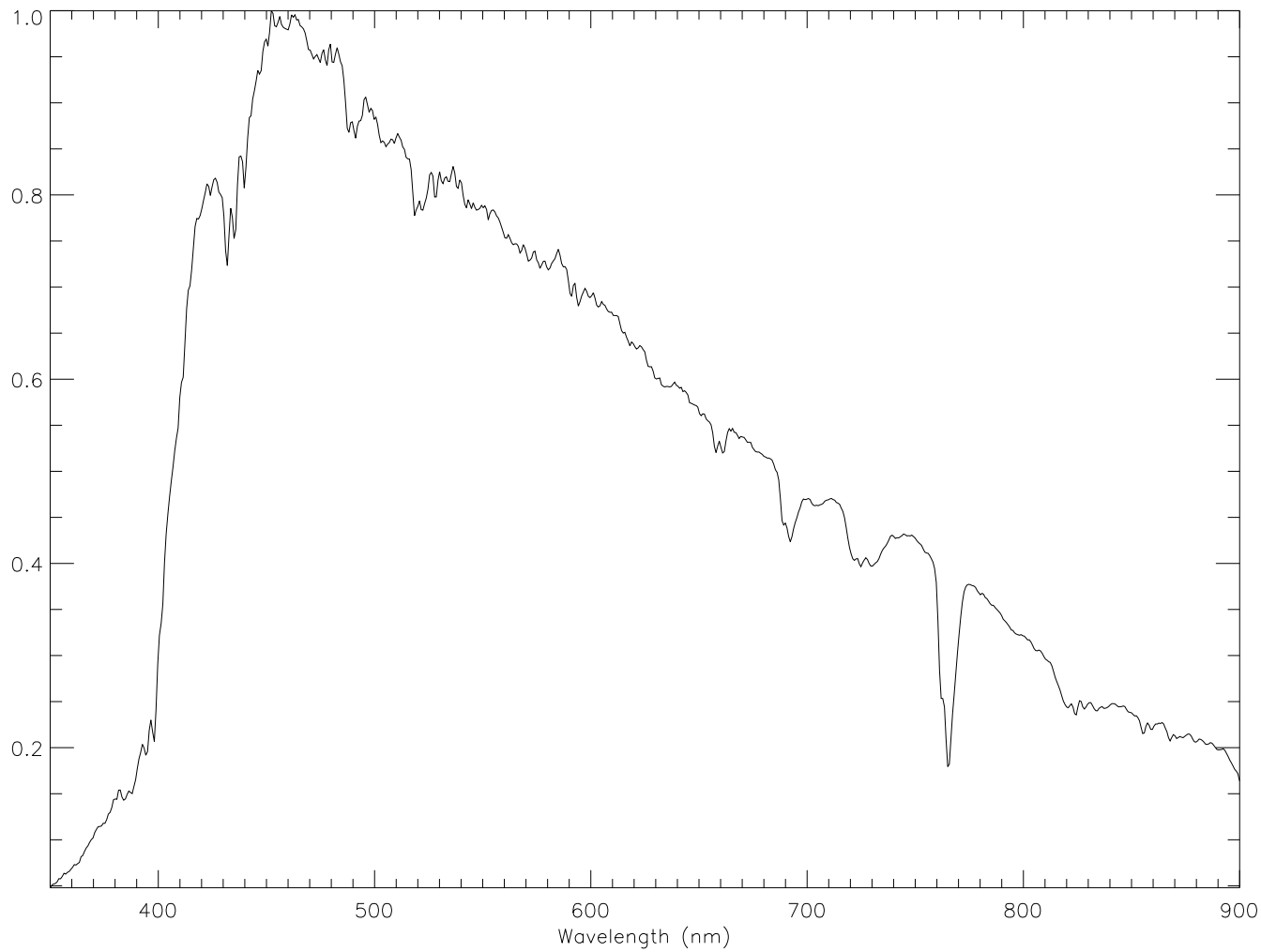


Fig. 16.— The pre-eclipse solar spectrum. Flux has been scaled by the maximum of the solar disk spectrum.

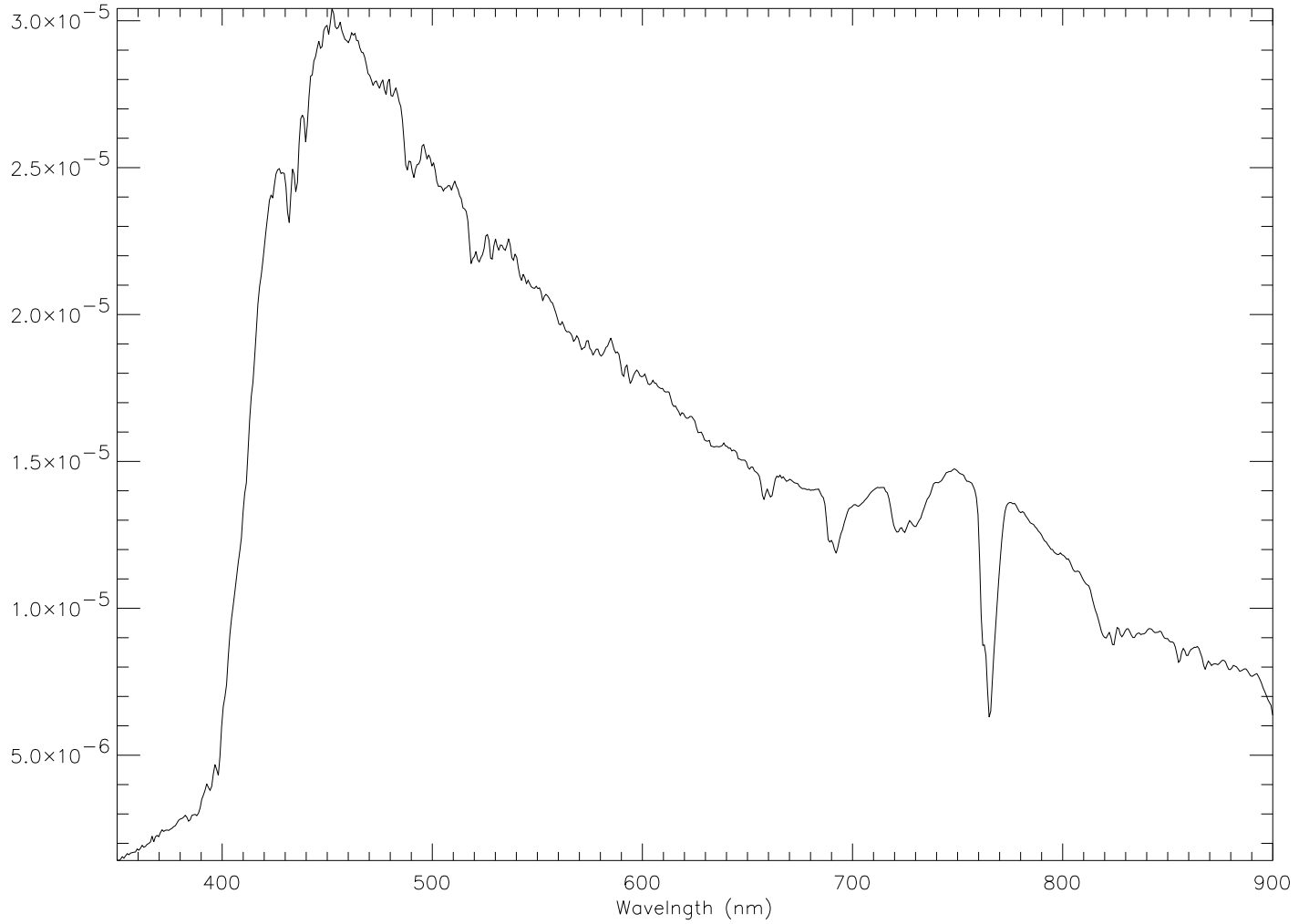


Fig. 17.— The pre-eclipse sky spectrum taken at a position of 45deg from zenith. Note the secondary maximum at 750 nm may be due to low lying dust in the atmosphere. Flux has been scaled by the maximum of the solar disk spectrum.

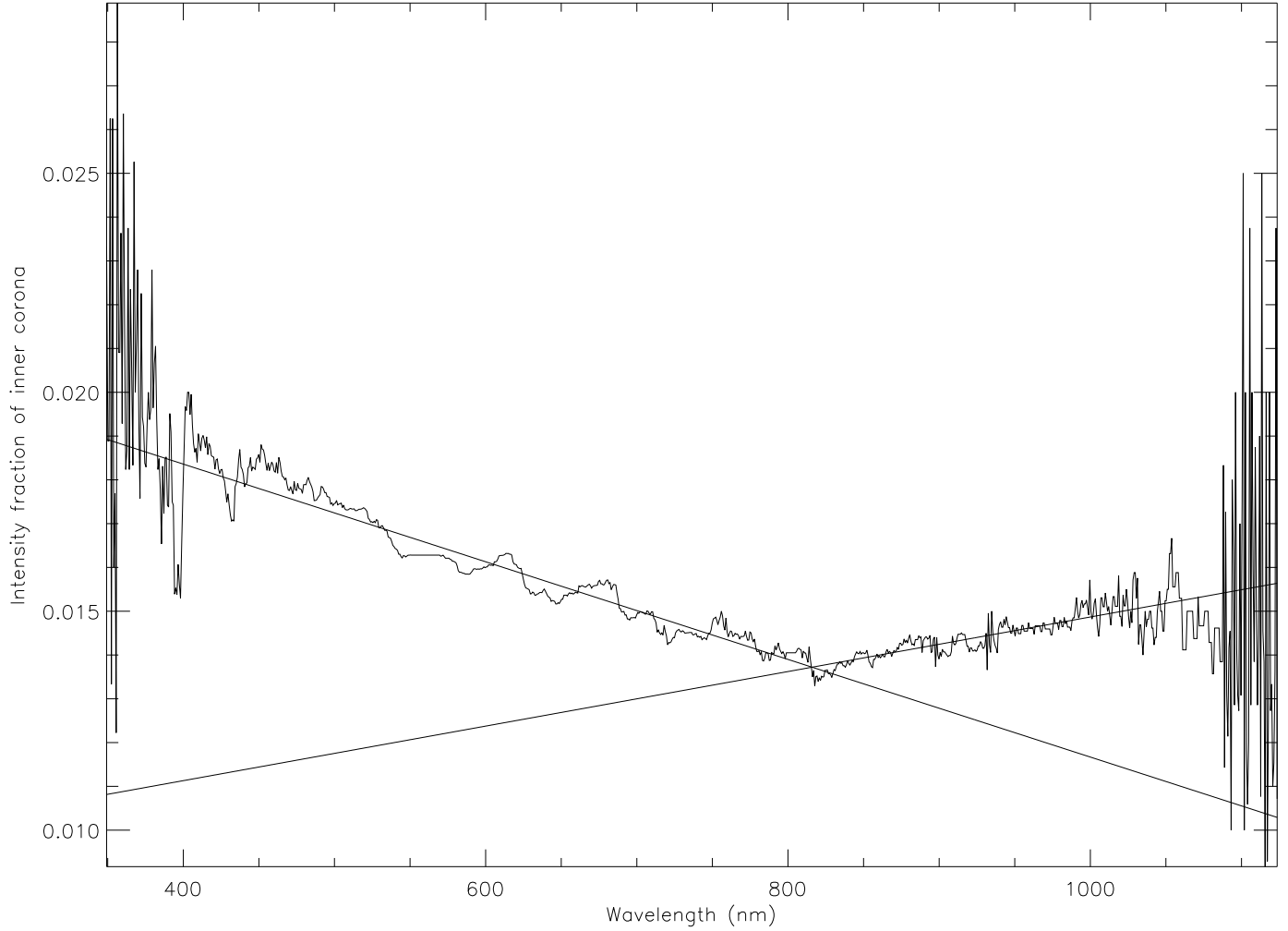


Fig. 18.— Median smoothing has been applied to the position 1 and 2 spectra, then position 2 is divided by position 1 yielding the relative flux difference versus wavelength, a basic measure of color. The ratio is characterized by two linear fits that are shown.

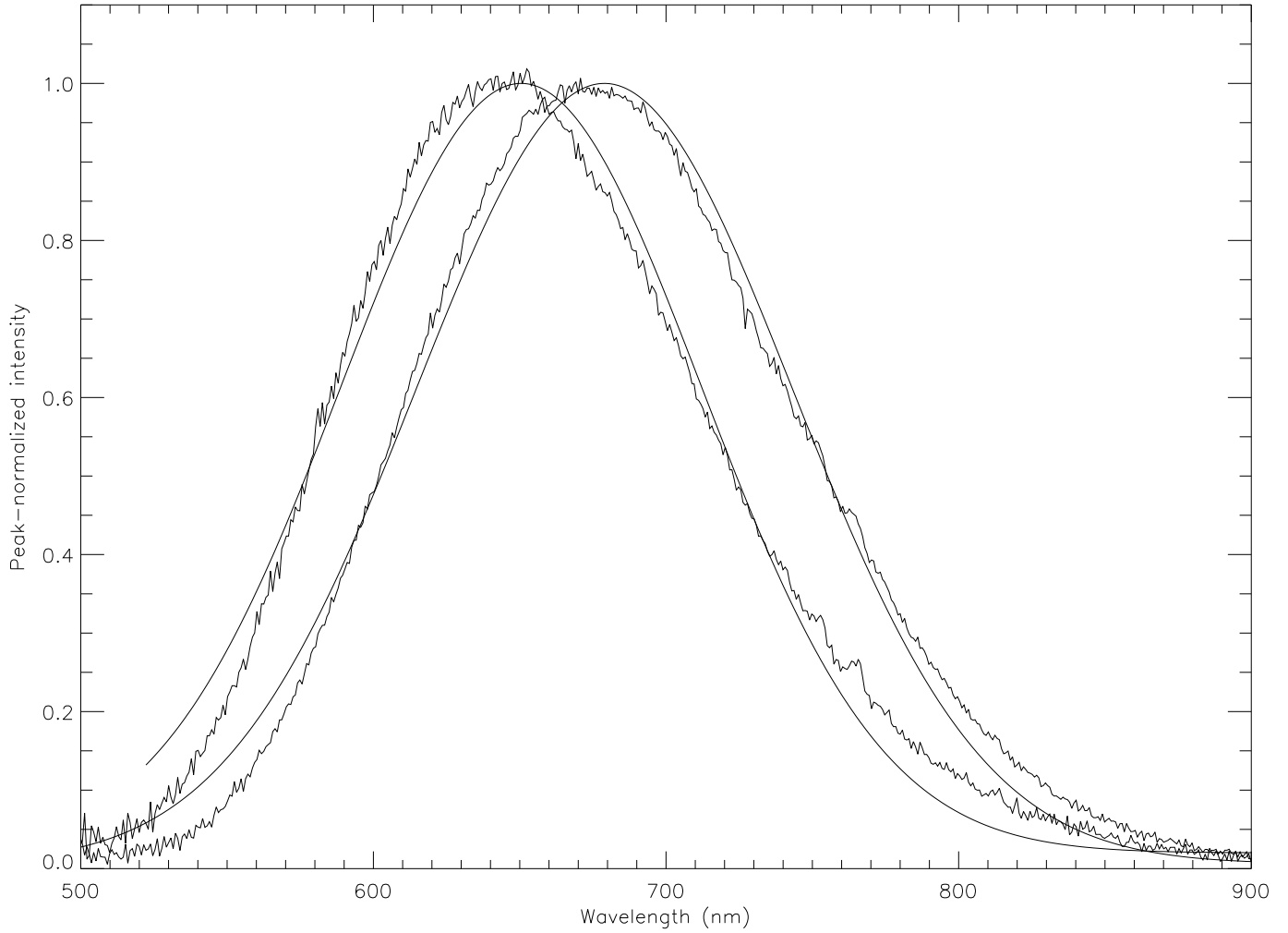


Fig. 19.— The visible wavelength silicon nanoparticle spectrum for the two samples, the sample with THF is on the left and the sample with ISO is on the right. Gaussian fits to the flux distribution have been overplotted.